

# Ferrofluid Simulations with the Barnes-Hut Algorithm on Graphics Processing Units

A. Yu. Polyakov<sup>a,b</sup>, T. V. Lyutyi<sup>a</sup>, S. Denisov<sup>b</sup>, V. V. Reva<sup>a</sup>, P. Hänggi<sup>b</sup>

<sup>a</sup>Sumy State University, Sumy, Ukraine

<sup>b</sup>Institute of Physics, University of Augsburg, Augsburg, Germany

---

## Abstract

We present an approach to molecular-dynamics simulations of dilute ferrofluids on graphics processing units (GPUs). Our numerical scheme is based on a GPU-oriented modification of the Barnes-Hut (BH) algorithm designed to increase the parallelism of computations. For an ensemble consisting of one million of ferromagnetic particles, the performance of the proposed algorithm on a Tesla M2050 GPU demonstrated a computational-time speed-up of four order of magnitude compared to the performance of the sequential All-Pairs (AP) algorithm on a single-core CPU, and two order of magnitude compared to the performance of the optimized AP algorithm on the GPU. The accuracy of the scheme is corroborated by comparing theoretical predictions with the results of numerical simulations.

*Keywords:* Ferrofluid, molecular dynamics simulation, the Barnes-Hut algorithm, GPUs, CUDA

---

## 1. Introduction

Ferrofluids are media composed of magnetic nanoparticles of diameters in the range 10÷50 nm which are dispersed in a viscous fluid (for example, water or ethylene glycol) [1]. These physical systems combine the basic properties of liquids, i.e. a viscosity and the presence of surface tension, and those of ferromagnetic solids possessing, i.e. an internal magnetization and high permeability to magnetic fields. The synergetic duality makes ferrofluids an attractive candidate for performing different tasks, ranging from the delivery of rocket fuel into spacecraft's thrust chambers under zero-gravity conditions to the high-precision drug delivery during cancer therapy [2]. Moreover, ferrofluids have already found its way into commercial applications as EM-controlled shock absorbers, dynamic seals in engines and computer hard-drives, and as a key element of high-quality loudspeakers, to name but a few [3].

Being liquids, ferrofluids can be modeled by using different macroscopic, continuum-media approaches. The corresponding field, ferrohydrodynamics [1], is a well-established area that has produced a lot of fundamental results. However, some important phenomena such as magnetoviscosity [4, 5], cannot be described properly neither on the hydrodynamical level nor within the single-particle picture [6]. The role of multiparticle aggregates – chains and clusters – appearing in the ferrofluid bulk, is important there. The insightful evaluation of other non-Newtonian features of ferrofluids, which can be controlled by external magnetic fields [5], also demands information about structure of aggregates and their dynamics. The key mechanism responsible for both is the dipole-dipole interaction acting between magnetic particles. Under certain conditions, the interaction effects can overcome the thermal fluctuations and start contribute tangibly to the ensemble dynamics. Therefore, in order to get a deeper insight into the above-mentioned features of ferrofluids, the interaction effects should be explicitly included into the modeling.

Strictly speaking, the dipole-dipole interaction acts between all the possible pairs of  $N$  ferromagnetic particles. Therefore, the computational time of the straightforward sequential algorithm scales like  $N^2$ . This is a fundamental drawback of many-body simulations and standard, CPU-based computational resources often limit the scales of the molecular-dynamics calculations. In order to run larger ensembles for longer times, researchers either (i) advance their models and numerical schemes and/or (ii) rely on more efficient computers. The first track led to different methods developed to explore the equilibrium properties of bulk ferrofluids. Most prominent are cut-off sphere approximations [7] or the Ewald summation technique [8], see also Ref. [9] for different modifications of the technique. However, both methods are of limited use for computational studies of confined ferrofluids, a problem that attracts special attention nowadays due to its practical relevance [10, 11]. An alternative approach is the search for new ways to increase

scalability and parallelism of computations, see Ref. [12]. Until recently, this practically meant the use of either large computational clusters, consisting of many Central Processing Units (CPUs) (Beowulf clusters and analogs) or massively parallel supercomputers, like Blue Gene supercomputers. The prices and the maintenance costs of such computational devices are high. The advent of the general-purpose computing on graphics processing units (GP<sup>2</sup>U) [13] has changed the situation drastically and boosted simulations of many-body systems onto a completely new level [14]. GPUs, initially designed to serve as the data pipelines for graphical information, are relatively small, relatively easy to maintain, and possess high computation capabilities allowing for parallel data processing. Nowadays, the scientific GPU-computing is used in many areas of computational physics, thanks to the Compute Unified Device Architecture (CUDA) developed by NVIDIA Corporation [15]. This step significantly simplified calculations so one could use a GPU as a highly-parallel computer directly, by programming it with *C*, *C++* or even *Fortran* [16] languages.

The typical scale of molecular-dynamics simulations in computational ferrofluid studies is within the range  $N = 10^2 - 10^3$  [17, 18], while  $N = 10^4$  constitutes the current limit [19]. It is evident that the increase of ensemble size by several orders of magnitude would drastically improve the statistical sampling and the quality of simulation results. To run numerically hundreds thousands (or even millions) of interacting magnetic particles is a task not much different from running an artificial Universe [20]. Therefore, similar to the case of Computational Cosmology [21, 22, 23], the GP<sup>2</sup>U seems to be very promising also in the context of ferrofluid simulations. In this paper we report the performance of a recently proposed GPU-oriented modification of the Barnes-Hut algorithm [24] for the simulation of the dynamics of  $N = 10^3 \div 10^6$  interacting ferromagnetic particles moving in a viscous medium.

Although being mentioned as a potentially promising approach (see, for example, Ref. [25]), the BH algorithm was never actually used for molecular-dynamics studies of ferrofluids, to the best of our knowledge. Our main goal here is to demonstrate a sizable speed-up one can reach when modeling such systems on a GPU – *and* by using GPU-oriented numerical algorithms – compared to the performance of conventional, CPU-based algorithms. We also demonstrate the high accuracy of the Barnes-Hut approximation by using the reduced magnetization vector as a benchmark. The paper is organized as follows: First, in Section II we specify the model. Then, in Section III, we describe how both, the All-Pairs and Barn-Hut algorithms, can be efficiently implemented for GPU-based simulations. The results of numerical tests are presented and discussed in Section V. Finally, Section VI contains conclusions.

## 2. The model

The model system represents an ensemble of  $N$  identical nanoparticles of the radius  $R$ , made of a ferromagnetic material with density  $D$  and having a specific magnetization  $\mu$ . Each particle occupies volume  $V = \frac{3}{4}\pi R^3$ , has magnetic moment  $\vec{m} = \vec{m}(t)$  (with the constant magnitude  $|\vec{m}| = m = V\mu$ ), mass  $M = VD$ , and moment of inertia  $I = \frac{2}{5}MR^2$ . The ensemble is dispersed in a liquid of viscosity  $\eta$ . Based on the Langevin dynamics approach, the equations of motions for  $k$ -th nanoparticle can be written in the following form [17]

$$I\ddot{\theta}_k = N_{kz} - G_r\dot{\theta}_k + \Xi_\theta^r, \quad (1)$$

$$I\ddot{\varphi}_k = -N_{kx} \sin \varphi_k + N_{ky} \cos \varphi_k - G_r\dot{\varphi}_k + \Xi_\varphi^r, \quad (2)$$

$$M\ddot{\vec{r}}_k = \mu_0(\vec{m}_k \nabla_k) \cdot \vec{H}_k + \vec{F}_k^{sr} - G_d\dot{\vec{r}}_k + \vec{\Xi}_k^d, \quad (3)$$

where  $\theta$  and  $\varphi$  are the polar and azimuthal angles of the vector  $\vec{m}$  respectively,  $N_{kx} = m_{ky}H_{kz} - m_{kz}H_{ky}$ ,  $N_{ky} = m_{kz}H_{kx} - m_{kx}H_{kz}$ ,  $N_{kz} = m_{kx}H_{ky} - m_{ky}H_{kx}$ ,  $x, y, z$  denotes the Cartesian coordinates, dots over the variables denote the derivatives with respect to time,  $G_t = 6\pi\eta R$ , and  $G_r = 8\pi\eta R^3$  are translational and rotational friction coefficients,  $\mu_0 = 4\pi \cdot 10^{-7}$  H/m is the magnetic constant,  $\vec{r}_k$  is the radius-vector, which define the nanoparticle position,  $\nabla_k = \frac{\partial}{\partial \vec{r}_k} = \vec{e}_x \frac{\partial}{\partial x_k} + \vec{e}_y \frac{\partial}{\partial y_k} + \vec{e}_z \frac{\partial}{\partial z_k}$ , ( $\vec{e}_x, \vec{e}_y, \vec{e}_z$  are the unit vectors of the Cartesian coordinates).  $\vec{H}_k$  is a resulting field acting on the of  $k$ -th

particle, and it is the sum of external field  $\vec{H}^{ext}$  and overall field exerted on the particle by the rest of the ensemble,

$$\vec{H}_k = \sum_{j=1, j \neq k}^N \vec{H}_{kj}^{dip} + \vec{H}^{ext}, \quad (4)$$

$$\vec{H}_{kj}^{dip} = \frac{3\vec{r}_{kj}(\vec{m}_j \vec{r}_{kj}) - \vec{m}_j \vec{r}_{kj}^2}{|\vec{r}_{kj}|^5}, \quad (5)$$

where  $\vec{r}_{kj} = \vec{r}_k - \vec{r}_j$ .  $\vec{F}_k^{sr}$  in Eq. 3 denotes the force induced by a short-range interaction potential. In this paper we use Lennard-Jones potential [17] (though hard sphere [26], soft sphere [27] and Yukawa-type [28] potentials can be used as alternatives), so that

$$\vec{F}_k^{sr} = 24E \sum_{j=1, j \neq k}^N \frac{\vec{r}_{kj}}{\vec{r}_{kj}^2} \left[ \left( \frac{s}{\vec{r}_{kj}} \right)^{12} - \left( \frac{s}{\vec{r}_{kj}} \right)^6 \right]. \quad (6)$$

Here  $E$  is the depth of the potential well and  $s$  is the equilibrium distance at which the inter-particle force vanishes. The interaction between a particle and container walls is also modeled with a Lennard-Jones potential of the same type. The random-force vector, representing the interaction of a particle with thermal bath, has standard white-noise components,  $\langle \Xi_\alpha^r(t) \rangle = 0$  ( $\alpha = \varphi, \theta$ ),  $\langle \Xi_\beta^d(t) \rangle = 0$  ( $\beta = x, y, z$ ), and second moments satisfying  $\langle \Xi_{r\alpha}(t) \Xi_{r\beta}(t') \rangle = 3k_B T G_r \delta_{\alpha\beta} \delta(t-t')$  ( $\alpha, \beta = \varphi, \theta$ )  $\langle \Xi_{d\alpha}(t) \Xi_{d\beta}(t') \rangle = 2k_B T G_t \delta_{\alpha\beta} \delta(t-t')$  ( $\alpha, \beta = x, y, z$ ) [17]. Here  $k_B$  is the Boltzmann constant and  $T$  is the temperature of the heat bath.

By rescaling the variables,  $\tau = t/T_{ch}$ , ( $T_{ch} = R/\mu \sqrt{3D/4\mu_0}$ ),  $\vec{u} = \vec{m}/|\vec{m}|$ ,  $\vec{\rho}_k = \vec{r}_k/R$ ,  $\nabla_{\rho_k} = \frac{1}{R} \frac{d}{d\rho_k}$ , the equations of motions for the  $k$ -th particle can be rewritten in the reduced form, to read:

$$\frac{2}{5} \cdot \frac{d^2 \theta_k}{d\tau^2} = (u_{kx} h_{ky} - u_{ky} h_{kx}) - \Gamma_r \frac{d\theta_k}{d\tau} + \frac{T_{ch}^2}{VR^2 D} \xi_\theta^r \quad (7)$$

$$\frac{2}{5} \cdot \frac{d^2 \varphi_k}{d\tau^2} = -(u_{ky} h_{kz} - u_{kz} h_{ky}) \sin \varphi_k + (u_{kz} h_{kx} - u_{kx} h_{kz}) \cos \varphi_k - \Gamma_r \frac{d\varphi_k}{d\tau} + \frac{T_{ch}^2}{VR^2 D} \xi_\varphi^r \quad (8)$$

$$\frac{d^2 \vec{\rho}_k}{d\tau^2} = \vec{f}_k^{dip} + \vec{f}_k^{sr} - \Gamma_d \frac{d\vec{\rho}_k}{d\tau} + \frac{T_{ch}^2}{VRD} \xi_{\vec{\rho}}^d \quad (9)$$

where

$$\vec{h}_k = \sum_{j=1, j \neq k}^N \vec{h}_{kj}^{dip} + \vec{h}^{ext}, \quad (10)$$

$$\vec{h}_{kj}^{dip} = \frac{3\vec{\rho}_{kj}(\vec{u}_j \vec{\rho}_{kj}) - \vec{u}_j \vec{\rho}_{kj}^2}{\rho_{kj}^5}, \quad (11)$$

$$\vec{f}_k^{dip} = \sum_{j=1, j \neq k}^N \left[ 3 \frac{\vec{\rho}_{kj}(\vec{u}_j \vec{u}_k) + \vec{u}_k(\vec{u}_j \vec{\rho}_{kj}) + \vec{u}_j(\vec{u}_k \vec{\rho}_{kj})}{\rho_{kj}^5} - 15 \frac{\vec{\rho}_{kj}(\vec{u}_k \vec{\rho}_{kj})(\vec{u}_j \vec{\rho}_{kj})}{\rho_{kj}^7} \right], \quad (12)$$

$$\vec{f}_k^{sr} = 24\varepsilon \sum_{j=1, j \neq k}^N \frac{\vec{\rho}_{kj}}{\rho_{kj}^2} \left[ \left( \frac{\sigma}{\rho_{kj}} \right)^{12} - \left( \frac{\sigma}{\rho_{kj}} \right)^6 \right], \quad (13)$$

Here  $\vec{h}^{ext} = 3\vec{H}^{ext}/4\pi\mu$ ,  $\Gamma_t = G_t T_{ch}/VD$ ,  $\Gamma_r = G_r T_{ch}/VR^2 D$ ,  $\sigma = s/R$ ,  $\varepsilon = ET_{ch}^2/VRD$ ,  $\vec{\rho}_{kj} = \vec{\rho}_k - \vec{\rho}_j$

Random-force vector's components are given now by white Gaussian noises, with the second moments satisfying  $\langle \xi_\alpha^r(\tau) \xi_\beta^r(\tau') \rangle = 3k_B T G_r \delta_{\alpha\beta} \delta(\tau-\tau')/T_{ch}$  ( $\alpha, \beta = \varphi, \theta$ )  $\langle \xi_\alpha^d(\tau) \xi_\beta^d(\tau') \rangle = 2k_B T G_t \delta_{\alpha\beta} \delta(\tau-\tau')/T_{ch}$  ( $\alpha, \beta = x, y, z$ ). In general case the characteristic relaxation time of particle magnetic moments to their equilibrium orientations is much smaller than  $T_{ch}$ , and one can neglect the magnetization dynamics by assuming that the direction of the vector  $\vec{m}_k$  coincides with the easy axis of the  $k$ -th particle. We assume that this condition holds for our model.

### 3. Two approaches to many-body simulations on GPUs: the All-Pairs and the Barnes-Hut algorithms

In this section we discuss two alternative approaches to the numerical propagation of the dynamical system given by Eqs. (7 - 9) on a GPU. It is assumed that the reader is familiar with the basics of the GP<sup>2</sup>U, otherwise we address him to Refs. ([29, 30]) that contain brief, crash-course-like introductions into the physically-oriented GPU computing.

#### 3.1. All-Pair Algorithm

The straightforward approach to simulations of a system of  $N$  interacting particles is to account for the interactions between all pairs. Although exact, the All-Pairs algorithm is slow when performed on a CPU, and it usually used to propagate systems of  $N = 10^2 \div 10^3$  particles. However, even with this simple approach one can tangibly benefit from GPUs by noticing that the All-Pairs algorithm fits CUDA architecture very well [31].

One integration step of the algorithm is performed in two stages. Namely,

1. Calculation of increment of particles' positions and magnetic moments directions.
2. Update particles' positions and magnetic moments directions.

This structure remains intact in the case of GPU computing. There is a need for the global synchronization of the threads that belong to the different blocks after every stage, the stages are performed on separate CUDA kernels and all the parameters of the system are kept in the global memory. The kernels responsible for the first stage compute forces that act on the particles, and calculate the corresponding increments for particles' positions and magnetic moments, according to the equations (7 - 9). The increments are then written into the global memory. Finally, second-stage kernels update the system state with the obtained increments.

Each thread is responsible for one particle of the ensemble, and thus it should account for the forces exerted on the particle by the rest of the ensemble. To speed up the computational process we keep the data vector of the thread particle in the shared memory, as well as the information on other particles, needed to compute the corresponding interaction forces. Thus we have two sets of arrays of data in the shared memory, namely

1. data of the particles assigned to the threads of the block;
2. data of particles to compute interaction with.

The necessary data are the coordinates of the particles, and projections of their magnetic moment vectors to  $x$ ,  $y$  and  $z$  axis. Size of the arrays are equal to number of threads per block. The first set of the data is constant during one integration step, but the second set is changed. So, at the beginning we upload the first set of particles' parameters to the second set of arrays in the shared memory. After computing the forces acting on the block particles (as it mention above the information on these particles is located in the first set of arrays in shared memory) the procedure is repeated, i. e. the parameter set another particles is written into the second set of arrays and the corresponding interactions are computed. The corresponding pseudo-code is presented the below. In the pseudo-code  $\Delta\rho_x, \Delta\rho_y, \Delta\rho_z, \Delta\theta, \Delta\varphi$  denote increments of a particle's coordinates  $x, y, z$ , and the direction angles of particle's magnetic moment,  $\theta$  and  $\varphi$ , needed to propagate the particle over one time step  $\Delta\tau$ .

The advantage of the described approach is that it uses the global memory in the most optimal way. The access to global memory is coalesced and there are no shared memory bank conflicts. For an ensemble  $N = 10^4$  particles this leads to computation utilization of 97.7%.

#### 3.2. Barnes-Hut Algorithm

The All-Pairs algorithm is simple and straightforward for implementation on GPU and perfectly fits CUDA. Yet this algorithm is purely scalable. The corresponding computation time grows like  $O(N^2)$ , and its performance is quite slow already for an ensemble of  $10^5$  particles.

The Barnes-Hut approximation [32] exhibits a much improved scalability and its computational time grows like  $O(N \log N)$ . The key idea of the algorithm is to substitute a group of particles with a single pseudo-particle mimicking the action of the group. Then the force exerted by the group on the considered particle can be replaced with the force exerted by the pseudo-particle. In order to illustrate the idea assume that all particles are located in a three-dimensional cube, which is named 'main cell'. The main cell is divided then into eight sub-cells. Each sub-cell confines subset of particles. If there are more than one particle in the given sub-cell then the last is again divided into eight sub-cells.

---

**Algorithm 1** A CUDA kernel that computes increments.

---

```

1: cached  $k \leftarrow \text{blockIdx}.x \cdot \text{blockDim}.x + \text{threadIdx}.x$ 
2: for  $j = 0$  to  $\text{numberOfParticles}$  do
3:   upload to shared memory particles positions and angles
4:   e.g.  $x_{\text{shared}}[\text{threadIdx}.x] = x_{\text{global}}[\text{ind}]$ , etc.
5:   for  $i = 0$  to  $\text{blockDim}.x$  do
6:     if  $j + i \neq k$  then ▷ the condition to avoid particle influence on self calculation
7:       Calculate force and dipole field the particle number  $j + i$ 
8:       on current  $k$ -th particle, and add the result to
9:       the total cached  $\vec{f}^{\text{dip}}$ ,  $\vec{f}^{\text{sr}}$ ,  $\vec{h}^{\text{dip}}$ .
10:    end if
11:  end for
12:  __syncthreads();
13:   $j \leftarrow j + \text{blockDim}.x$ 
14: end for
15: Calculation of cached  $\Delta\rho_x, \Delta\rho_y, \Delta\rho_z, \Delta\theta, \Delta\varphi$  according to equations 7 - 9.
16: Copy increments to global memory.

```

---

The procedure is re-iterated until there are only one or none particles left in each sub-cell. In this way we can obtain an octree with leaves that are either empty or contain single particle only. A simplified, two-dimensional realization of this algorithm is sketched with Fig. 1.

Thus, by following the above-given recipe, we assign to every cell, obtained during the decomposition, a pseudo-particle, with magnetic moment  $\vec{u}'$  equals to the sum of magnetization vectors  $\vec{u}$  of the particles belonging to the cell, and position  $\vec{\rho}'$  which is the position of the geometrical center of the sub-set,

$$\vec{\rho}' = \frac{\sum_{i=1}^{N'} \vec{\rho}_i}{N'}, \quad (14)$$

where  $N'$  is a number of particles in the cell and  $\vec{\rho}_i$  is the position of the  $i$ -th particle from the sub-set.

Forces acting on  $k$ -th particle can be calculated by traversing the octree. If the distance from the particle to the pseudo-particle, that is correspond to the root cell, is large enough, the influence of this pseudo-particle on the  $k$ -th particle is calculated; otherwise pseudo-particles of the next sub-cells are checked etc (sometime this procedure can lead finally to a leaf with only one particle in the cell left). Thus calculated force is added then to the total force acting on the  $k$ -th particle.

The Barnes-Hut algorithm allows for a high parallelism of computations and it is widely employed in computational astrophysics problems [33]. However, implementation of the Barnes-Hut algorithm on GPUs remained a challenge until recently. This is so because the procedure uses an irregular tree structure that does not fit the architecture of CUDA well. This is the reason why the Barnes-Hut idea was not realized entirely on a GPU but some part of calculations was delegated and performed on a CPU [34, 35]. A realization of the algorithm solely on a GPU has been proposed only in 2011 [24]. Below we briefly outline the main idea of the proposal.

In contrast to the All-Pairs algorithm, where only two kernels were involved, in this case one needs six kernels [24]:

1. Bounding box definition kernel.
2. Octree building kernel.
3. Computing geometrical center and total magnetic moment of each cell.
4. Sorting of the particles with respect to their positions.
5. Computing forces and fields acting on each particle.
6. Integration kernel.

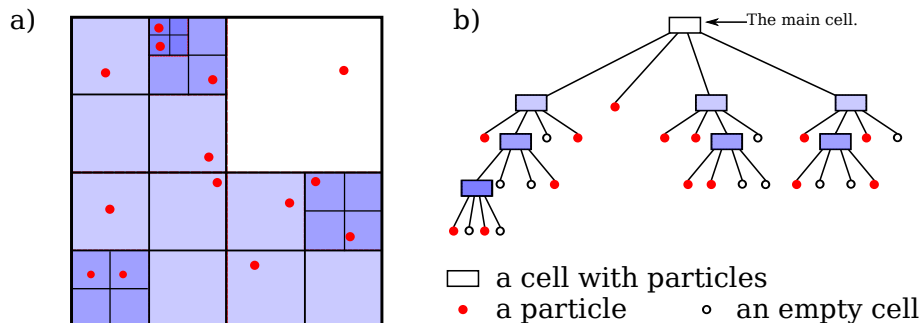


Figure 1: Barnes-Hut hierarchical decomposition in two-dimensional space and the corresponding octree. See Section 3.2 for more details.

$N$	$AP_{CPU}$	$AP_{GPU}$	$BH_{GPU}$	$\frac{AP_{CPU}}{AP_{GPU}}$	$\frac{AP_{CPU}}{BH_{GPU}}$	$\frac{AP_{GPU}}{BH_{GPU}}$
$10^3$	34	0.7	2	49	17	0.35
$10^4$	3 470	20	6.5	174	534	3.1
$10^5$	392 000	1 830	54	214	7 259	33.9
$10^6$	39 281 250	184 330	621	213	63 214	297

Table 1: Duration of single integration step (ms) for the optimized All-Pairs algorithm implemented on CPU ( $AP_{CPU}$ ) and GPU ( $AP_{GPU}$ ), and for the GPU-oriented Barnes-Hut algorithm ( $BH_{GPU}$ ).

The kernel 1 defines the boundaries of the root cell. Since we always assumed that the ensemble is confined to a container and particles cannot go outside, we decided to leave this kernel following the recommendation given in Ref. [24] for the case when particles density is heterogeneous. In this case size of the root cell can be significantly smaller than the characteristic size of the container. Moreover, the computation time of this kernel is very small, typically much less than 1% of the total time of one integration step. The kernel 2 performs hierarchical decomposition of the root cell and builds an “octree in the three dimensional case. For two dimensions the situation is depicted with a “quadtree, as depicted with Fig. 1. The kernel 3 computes magnetic moment and position of pseudo-particles associated with cells. Kernel 4 sorts particles according to their locations. This step can significantly speed up computations due to the optimal global memory access. Kernel 5 computes forces acting on the particles, and then calculates the corresponding increments. Finally, the kernel 6 updates the state of the particles. We direct the interested reader to Ref. [24] for more detailed description of the algorithm.

## 4. Results

We performed simulations on (i) a PC with Intel Xeon x5670 @2.93GHz CPU(48 Gb RAM) and (ii) a Tesla M2050 GPU. Though the CPU has six cores, only a single core was used in simulations. The programs were compiled with `nvcc` (version 4.0) and `gcc` (version 4.4.1) compilers. Since there was no need in high-precision calculations, we used single-precision variables (`float`) and compiled the program with `-use_fast_math` key. We also used `-O3` optimization flag to speedup our programs. Finally, the Euler-Maruyama method with time step  $\Delta\tau = 0.001$  was used to integrate Eq. (7 - 9).

We measured the computation time of one integration step for both algorithms as functions of  $N$ . The results are presented with Table 1. The benefits of the GPU computing increase with the number of particles. For an ensemble of  $N = 10^6$  particles the speed-up gained by the use of the Barnes-Hut algorithm is almost 300 compared to the performance of the optimized All-Pairs algorithm on the same GPU. However, for  $N = 10^3$  the All-Pairs algorithm performs better. It is because for small numbers of particles the computational expenses for the tree-building phase, sorting etc., overweight the speed-up effect of the approximation. We remind that  $N = 10^3$  was the typical scale of the most of ferrofluidic simulations to date [17, 18], and, although being classified as a potentially useful approach (see e.g. in Ref. [25]), the BH algorithm was never implemented for molecular-dynamics studies of ferrofluids before, to the best of our knowledge.

Fig. 2 shows instantaneous configurations obtained during the simulations for a cubic confinement and for a mono-layer. To simulate a mono-layer of particles we use a parallelepiped of the height  $2.1R$  as a confinement. The parameters of the simulations correspond to the regime when the average dipole energy is much larger than the energy of thermal fluctuations. The formation of chain-like large-scale clusters [36] is perfectly visible.

### 5. A benchmark test: average magnetization curves

In order to check the accuracy of the numerical schemes we calculated the reduced magnetization curve [36]. Reduced magnetization vector is given by the sum  $\langle \vec{u} \rangle = 1/N \sum_{i=1}^N \vec{u}_i$ . The main parameters that characterize a ferrofluid are the dipole coupling constant  $\lambda$ , which is the ratio of dipole-dipole potential and thermal energy, namely [37],

$$\lambda = \frac{\mu_0 m^2}{16\pi R^3 k_B T}, \quad (15)$$

and the volume fraction, which is the ratio between the volume occupied by particles and the total volume occupied by the ferrofluid,  $V_f$ , i.e.,

$$\phi = \frac{4/3\pi R^3 N}{V_f} \cdot 100\%. \quad (16)$$

In the limit when  $\lambda < 1$  and for small volume fraction,  $\phi \ll 100\%$ , the projection of the reduced magnetization vector on the direction of applied field,  $\langle u_{\vec{H}} \rangle$ , can well be approximated by the Langevin function [36]:

$$\langle u_{\vec{H}} \rangle = L(\alpha) = \coth(\alpha) - \frac{1}{\alpha}, \quad (17)$$

where  $\alpha$  denotes the ratio between magnetic energy and thermal energy,  $\alpha = m\mu_0 H/k_B T$ .

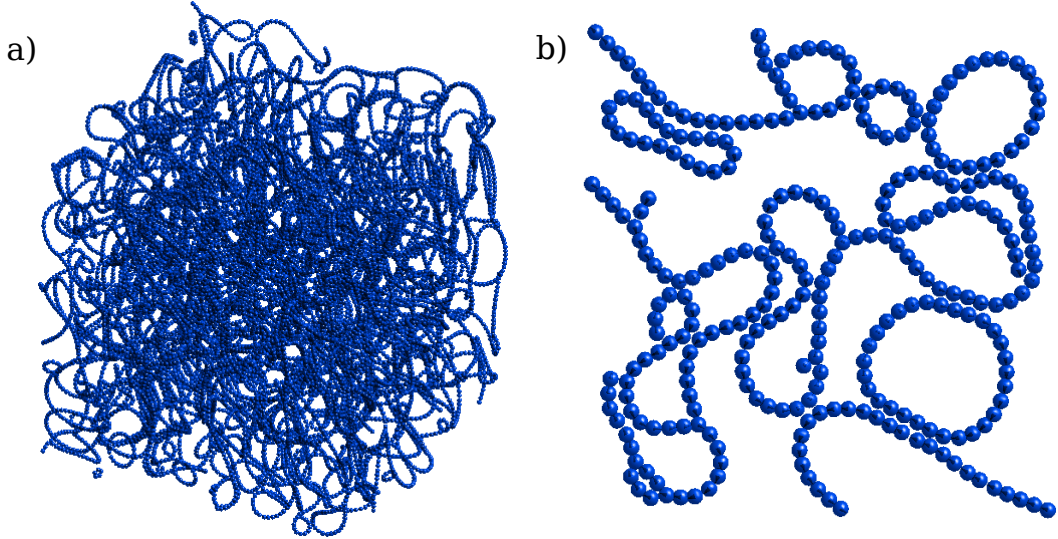


Figure 2: Snapshots of  $N$ -particle ensembles obtained with the Barnes-Hut algorithm: (a)  $N = 20\,000$  (cubic confinement with the edge length  $L = 150R$ ) and (b) mono-layer of  $N = 300$  particles. The parameters are:  $\Gamma_r = \Gamma_t = 0.1$ ,  $T = 300$  K,  $\mu = 3.1 \cdot 10^5$  A/m,  $D = 5000$  kg/m<sup>3</sup>,  $R = 10$  nm.

We simulated a system with the parameters corresponding to maghemite ( $\gamma\text{-Fe}_2\text{O}_3$ ) with a saturation magnetization of  $\mu = 3.1 \cdot 10^5$  A/m and density  $D = 5000$  kg/m<sup>3</sup>, the carrier viscosity  $\eta = 0.89 \cdot 10^{-3}$  Pa (the latter corresponds to the water viscosity at  $T = 298$  K). The volume fraction is set at  $\phi = 1\%$  and the particle radius  $R = 3$  nm. The

external magnetic field  $\vec{H}$  was applied along  $z$ -axis. We initiated the system at time  $\tau = 0$  by randomly distributing particles in a cubic container. The orientations of particle magnetization vectors were obtained by drawing random values for the orientation angles from the interval  $[0, 2\pi]$ .

Fig. 3 presents the results of the simulations. After the transient  $\tau_{eq} = 1000$ , given to the system of  $N = 10^5$  particles to equilibrate, the mean reduced magnetization has been calculated by averaging  $\langle u_z \rangle$  over the time interval  $\tau_{calc} = 1000$ . It is noteworthy that even single-run results are very close to the Langevin function, see Fig. 3(a). The contribution of the magnetostatic energy grows with  $\alpha$  so that the strength of the dipole-dipole interaction is also increasing, see Fig. 4.

Since the average value of dipole field projection on  $z$  axis is positive and increases with  $\alpha$  (see Fig. 4), the dipole field amplify the external one. It leads to additionally alignment in the ensemble and explains the discrepancy between the analytical and numerical results obtained for large values of  $\alpha$ . For an ensemble of  $N = 10^3$  particles the results obtained with two algorithms are near identical, Fig. 3 (b).

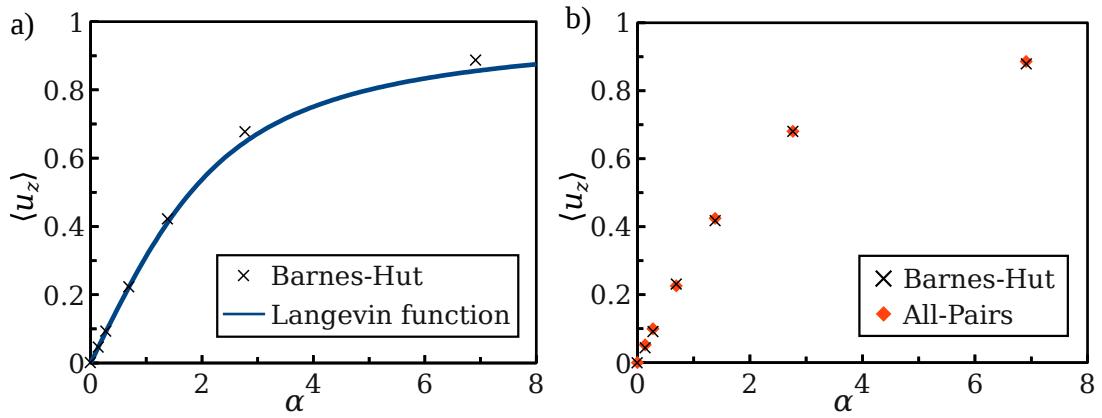


Figure 3: Checking the Barnes-Hut approximation: a) comparison between the single-run results obtained with  $N = 10^5$  particles and Langevin function, Eq. (17); b) comparison of the results obtained with the All-Pair and the Barnes-Hut algorithms for  $N = 10^3$  particles.

It is important also to compare the average dipole fields,  $\langle h_z^{dip} \rangle$ , calculated with the Barnes-Hut and the All-Pairs algorithms. The results obtained for the above-given set of parameters are shown on Fig.4. Again, two algorithms produced almost identical results.

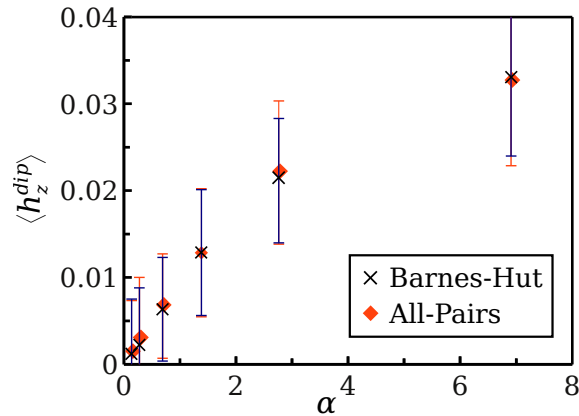


Figure 4:  $z$ -component of the reduced average dipole field as a function of  $\alpha$  calculated with two different algorithms. The parameters are the same as in Fig. 3(b). Each point was obtained by averaging over 1000 realizations.

## 6. Conclusions

With this work we demonstrated that the Barnes-Hut algorithm can be efficiently implemented for large-scale, GPU-based ferrofluid simulations. Overall, we achieved a speed-up more than two orders of magnitude when compared to the performance of a common GPU-oriented All-Pairs algorithm. The proposed approach allows to increase the size of ensembles by two orders of magnitude compared to the present-day scale of simulations [19]. The Barnes-Hut algorithm correctly accounts for the dipole-dipole interaction within an ensemble of  $N = 10^6$  particles and produces results that fit the theoretical predictions with high accuracy. Our finding opens several interesting future perspectives. First, it brings about possibilities to perform large-scale molecular-dynamics simulations for the time evolution of ferrofluids placed in confinements of complex shapes like thin vessels or tangled pipes, where the boundary effects play an important role [38]. It is also possible to explore the *non-equilibrium* dynamics of ferrofluids, for example, their response to different types of externally applied magnetic fields, such as periodically alternating fields [39], or gradient fields [40]. Another direction for further studies is the exploration of the relationship between shape and topology of nano-clusters and different macroscopic properties of ferrofluids [41, 42]. Finally, the proposed method here allows to study heat transport processes in ferrofluids [43], as well as the study of the performance of ferromagnetic particles acting as heat sources in the context of magnetic fluid hyperthermia [44].

## 7. Acknowledgment

A.Yu.P. and T.V.L. acknowledge the support of the Cabinet of Ministers of Ukraine obtained within the Program of Studying and Training for Students, PhD Students and Professor's Stuff Abroad and the support of the Ministry of Education, Science, Youth, and Sport of Ukraine (Project No 0112U001383). S.D. and P.H. acknowledge the support by the cluster of excellence Nanosystems Initiative Munich (NIM).

## References

- [1] R. Rosensweig, *Ferrohydrodynamics*, Cambridge University Press, 1985.
- [2] Q. Pankhurst, J. Connolly, S. Jones, J. Dobson, Applications of magnetic nanoparticles in biomedicine, *J. Phys. D Appl. Phys.* 36 (2003) R167.
- [3] K. Raj, R. Moskowitz, Commercial applications of ferrofluids, *J. Magn. Magn. Mater.* 85 (1990) 233.
- [4] J. P. McTague, Magnetoviscosity of magnetic colloids, *J. Chem. Phys.* 51 (1969) 133.
- [5] S. Odenbach, *Magnetoviscous effects in ferrofluids*, Springer, 2002.
- [6] S. Odenbach, H. Stoerk, Shear dependence of field-induced contributions to the viscosity of magnetic fluids at low shear rates, *J. Magn. Magn. Mater.* 183 (2000) 188.
- [7] P. Ilg, E. Coquelle, S. Hess, Structure and rheology of ferrofluids: simulation results and kinetic models, *J. Phys. Condens. Mat.* 18 (2006) S2757.
- [8] S. de Leeuw, J. Perram, E. Smith, Simulation of Electrostatic Systems in Periodic Boundary Conditions. I. Lattice Sums and Dielectric Constants, in: *Proc. R. Soc. Lond. A Math. Phys. Sci.*, volume 373, 1980, p. 27.
- [9] J. J. Cerdà, V. Ballenegger, O. Lenz, C. Holm, P3M algorithm for dipolar interactions., *J. Chem. Phys.* 129 (2008) 234104.
- [10] H. Hartshorne, C. J. Backhouse, W. E. Lee, Ferrofluid-based microchip pump and valve, *Sensor. Actuat. B Chem.* 99 (2004) 592.
- [11] N. Pamme, Magnetism and microfluidics, *Lab Chip* 6 (2006) 24.
- [12] J. Phillips, R. Braun, W. Wang, et al., Scalable Molecular Dynamics with NAMD, *J. Comput. Chem.* 26 (2005) 1781.
- [13] J. D. Owens, D. Luebke, N. Govindaraju, M. Harris, J. Krüger, A. E. Lefohn, T. J. Purcell, A Survey of GeneralPurpose Computation on Graphics Hardware, *Comput. Graph. Forum* 26 (2007) 80.
- [14] L. Nyland, M. Harris, J. Prins, Fast N-body simulation with CUDA, *GPU Gems 3*, edited by H. Nguyen, chap. 31 (2007).
- [15] J. Sanders, E. Kandrot, *CUDA by Examples*, Addison-Wesley, 2011.
- [16] *CUDA Fortran Programming Guide and Reference*, 2012. URL: <http://www.pgroup.com/lit/whitepapers/pgicudaforug.pdf>.
- [17] Z. Wang, C. Holm, H.-W. Müller, Molecular dynamics study on the equilibrium magnetization properties and structure of ferrofluids, *Phys. Rev. E* 66 (2002) 021405.
- [18] A. O. Ivanov, S. S. Kantorovich, E. N. Reznikov, et al., Magnetic properties of polydisperse ferrofluids: A critical comparison between experiment, theory, and computer simulation, *Phys. Rev. E* 75 (2007) 061405.
- [19] J. J. Cerdà, E. Efimova, V. Ballenegger, E. Krutikova, A. Ivanov, C. Holm, Behavior of bulky ferrofluids in the diluted low-coupling regime: Theory and simulation, *Phys. Rev. E* 81 (2010) 011501.
- [20] V. Springel, S. D. M. White, A. Jenkins, C. S. Frenk, N. Yoshida, L. Gao, J. Navarro, R. Thacker, D. Croton, J. Helly, J. A. Peacock, S. Cole, P. Thomas, H. Couchman, A. Evrard, J. Colberg, F. Pearce, Simulations of the formation, evolution and clustering of galaxies and quasars, *Nature* 97 (2005) 629.
- [21] S. F. P. Zwart, R. G. Bellemana, P. M. Geldofa, High-performance direct gravitational N-body simulations on graphics processing units, *New Astron.* 12 (2007) 641.

- [22] R. G. Belleman, J. Bédorf, S. F. P. Zwart, High performance direct gravitational N-body simulations on graphics processing units II: An implementation in CUDA, *New Astron.* 13 (2008) 103.
- [23] D. Aubert, Numerical Cosmology powered by GPUs, in: *Proceedings of the International Astronomical Union*, volume 6, 2010, p. 397.
- [24] M. Bartscher, K. Pingali., An Efficient Cuda Implementation of the Tree-based Barnes Hut N-body Algorithm, in: *GPU Gems '11: GPU Computing Gems Emerald Edition*, 2011.
- [25] C. Holm, Efficient Methods for Long Range Interactions in Periodic Geometries Plus One Application, in: *Computational Soft Matter: From Synthetic Polymers to Proteins*, Research Centre Julich, 2004.
- [26] J. Weis, D. Levesque, Chain formation in low density dipolar hard spheres: A Monte Carlo study, *Phys. Rev. Lett.* 71 (1993) 2729–2732.
- [27] D. Wei, G. Patey, Orientational order in simple dipolar liquids: Computer simulation of a ferroelectric nematic phase, *Phys. Rev. Lett.* 68 (1992) 2043–2045.
- [28] G. Mériguet, M. Jardat, P. Turq, Brownian dynamics investigation of magnetization and birefringence relaxations in ferrofluids., *J. Chem. Phys.* 123 (2005) 144915.
- [29] M. Januszewski, M. Kostur., Accelerating numerical solution of stochastic differential equations with cuda, *Comput. Phys. Commun.* 181 (2010) 183.
- [30] M. Weigel, Simulating spin models on GPU, *Comput. Phys. Commun.* 182 (2011) 1833.
- [31] H. Nguyen, *Gpu gems 3*, first ed., Addison-Wesley Professional, 2007.
- [32] J. Barnes, P. Hut, A hierarchical  $O(N \log N)$  force-calculation algorithm, *Nature* 324 (1986) 446–449. doi:10.1038/324446a0.
- [33] J. Barnes, *Computational Astrophysics*, Berlin: Springer-Verlag, 1994.
- [34] E. Gaburov, J. Bédorf, S. P. Zwart, Gravitational tree-code on graphics processing units: implementation in CUDA, *Procedia Comput. Sci.* 1 (2010) 1119–1127.
- [35] H. Jiang, Q. Deng, Barnes-Hut treecode on GP, in: *2010 IEEE International Conference on Progress in Informatics and Computing (PIC)*, volume 2, 2010, pp. 974–978. doi:10.1109/PIC.2010.5687868.
- [36] M. Shliomis, Magnetic fluids, *Sov. Phys. Usp.* 17 (1974) 153.
- [37] A. Wang, J. Li, R. Gao, The structural force arising from magnetic interactions in polydisperse ferrofluids, *Appl. Phys. Lett.* 94 (2009) 2009–2011.
- [38] Z. Wang, C. Holm, H. W. Müller, Boundary condition effects in the simulation study of equilibrium properties of magnetic dipolar fluids, *J. Chem. Phys.* 119 (2003) 379–387.
- [39] T. Mahr, I. Rehberg, Nonlinear dynamics of a single ferrofluid-peak in an oscillating magnetic field, *Physica D* 111 (1998) 335–346.
- [40] R. M. Erb, D. S. Sebba, A. A. Lazarides, B. B. Yellen, Magnetic field induced concentration gradients in magnetic nanoparticle suspensions: Theory and experiment, *J. Appl. Phys.* 103 (2008) 063916.
- [41] V. S. Mendelev, A. O. Ivanov, Ferrofluid aggregation in chains under the influence of a magnetic field, *Phys. Rev. E* 70 (2004) 051502.
- [42] D. Borin, A. Zubarev, D. Chirikov, R. Müller, S. Odenbach, Ferrofluid with clustered iron nanoparticles: Slow relaxation of rheological properties under joint action of shear flow and magnetic field, *J. Magn. Magn. Mater.* 323 (2011) 1273–1277.
- [43] R. Ganguly, S. Sen, I. K. Puri, Heat transfer augmentation using a magnetic fluid under the influence of a line dipole, *J. Magn. Magn. Mater.* 271 (2004) 63–73.
- [44] R. Rosensweig, Heating magnetic fluid with alternating magnetic field, *J. Magn. Magn. Mater.* 252 (2002) 370–374.